

Green Polymer Electrolytes Based on Polycaprolactones for Solid-State High-Voltage Lithium Metal Batteries

Yi-Hsuan Chen, Yi-Chen Hsieh, Kun Ling Liu, Lennart Wichmann, Johannes Helmut Thienenkamp, Aditya Choudhary, Dmitry Bedrov, Martin Winter, and Gunther Brunklaus*

Solid polymer electrolytes (SPEs) have attracted considerable attention for high energy solid-state lithium metal batteries (LMBs). In this work, potentially ecofriendly, solid-state poly(€-caprolactone) (PCL)-based star polymer electrolytes with cross-linked structures (xBt-PCL) are introduced that robustly cycle against LiNi_{0.6}Mn_{0.2}Co_{0.2}O₂ (NMC622) composite cathodes, affording long-term stability even at higher current densities. Their superior features allow for sufficient suppression of dendritic lithium deposits, as monitored by ⁷Li solid-state NMR. Advantageous electrolyte|electrode interfacial properties derived from cathode impregnation with 1.5 wt% PCL enable decent cell performance until up to 500 cycles at rates of 1C (60 °C), illustrating the high potential of PCL-based SPEs for application in high-voltage LMBs.

1. Introduction

As essential component within lithium-based batteries, the electrolyte plays a vital role for achieving long-term electrochemical performance and safety. Despite their potential in providing high specific capacity, current lithium metal batteries (LMBs) are eventually limited by inhomogeneous lithium deposition (high-surface area lithium (HSAL)) or disadvantageous

Y.-H. Chen, Y.-C. Hsieh, K. L. Liu, L. Wichmann, J. H. Thienenkamp, M. Winter, G. Brunklaus
Helmholtz Institute Münster|IEK-12
Forschungszentrum Jülich GmbH
Corrensstraße 46, 48149 Münster, Germany
E-mail: g.brunklaus@fz-juelich.de
A. Choudhary, D. Bedrov
Department of Materials Science and Engineering
University of Utah
122 S. Central Campus Dr., Salt Lake City, UT 84112, USA
M. Winter
MEET Battery Research Center
Institute of Physical Chemistry
University of Münster
Corrensstraße 46, 48149 Münster, Germany

The ORCID identification number(s) for the author(s) of this article can be found under https://doi.org/10.1002/marc.202200335

© 2022 The Authors. Macromolecular Rapid Communications published by Wiley-VCH GmbH. This is an open access article under the terms of the Creative Commons Attribution License, which permits use, distribution and reproduction in any medium, provided the original work is properly cited.

DOI: 10.1002/marc.202200335

flammability arising from organic liquid electrolytes. [1-6] In contrast, solid-state electrolytes, including organic- (polymers) and inorganic-based (oxides and sulfides) materials, are introduced as alternatives for highenergy density LMBs affording enhanced safety and sufficient mechanical stability against lithium dendrite formation.[7,8] Though many ceramic materials exhibit good ionic conductivity, their high costs of both synthesis and raw materials and the effortful conditions for membrane processing yet restrict large-scale production.[7,9] In contrast, solid polymer electrolytes (SPEs) represent suitable candidates for industrial applications, owing to their good processability, mechanical flexibility as well as

reasonable costs. [10-12] To date, poly (ethylene oxide) (PEO)-based SPEs were extensively studied among many other polymer hosts, attributed to their large-scale availability and superior solvation ability with Li-ions.[13] The latter, however, significantly reduces later release of Li-ions, thus yielding rather poor Li-ion transference numbers (t_+) in the range of 0.1-0.2. This may contribute to the occurrence of concentration polarization within the cells and to elevated interfacial resistances and inadequate longterm cycling performance.[13,15] Though PEO, unlike typical liquid organic carbonate-based electrolytes, exhibits no significant oxidation reactions at potentials of up to 4.6 V versus Li|Li+, it may suffer from strong capacity-fading upon long-term cell operation, reflecting continuous oxidative degradation at higher operation temperature (60 °C) that limit its applications toward practical high-voltage cathodes. In contrast, long-term compatibility and robust cycling stability against low-voltage LiFePO₄ (LFP) has been successfully shown.[11,16-18]

Urged by environmental impacts, intensive research focusses on the development of "greener" materials within lithium based batteries to promote the sustainability of the cells throughout the whole life cycle, yet less attention is paid to solid polymer electrolytes. [19,20] As a promising alternative to PEO, poly(ϵ -caprolactone) (PCL)-based SPEs have gained scientific attention in recent years, motivated by its biocompatibility, wide electrochemical stability window (5 V vs Li|Li+) and comparatively high Li-ion transference number ($t_+ > 0.5$). [21,22] Note that upon Lisalt addition, PCL with reduced crystalline phase allowed for full biodegradation after only 110 days in soil compost, demonstrating high potential of sustainability for this class of SPEs. [20]





Table 1. Electrochemical performances of various PCL-based[23-25] and cross-linked PEO-based[28-30] high-voltage cell systems reported in literature.

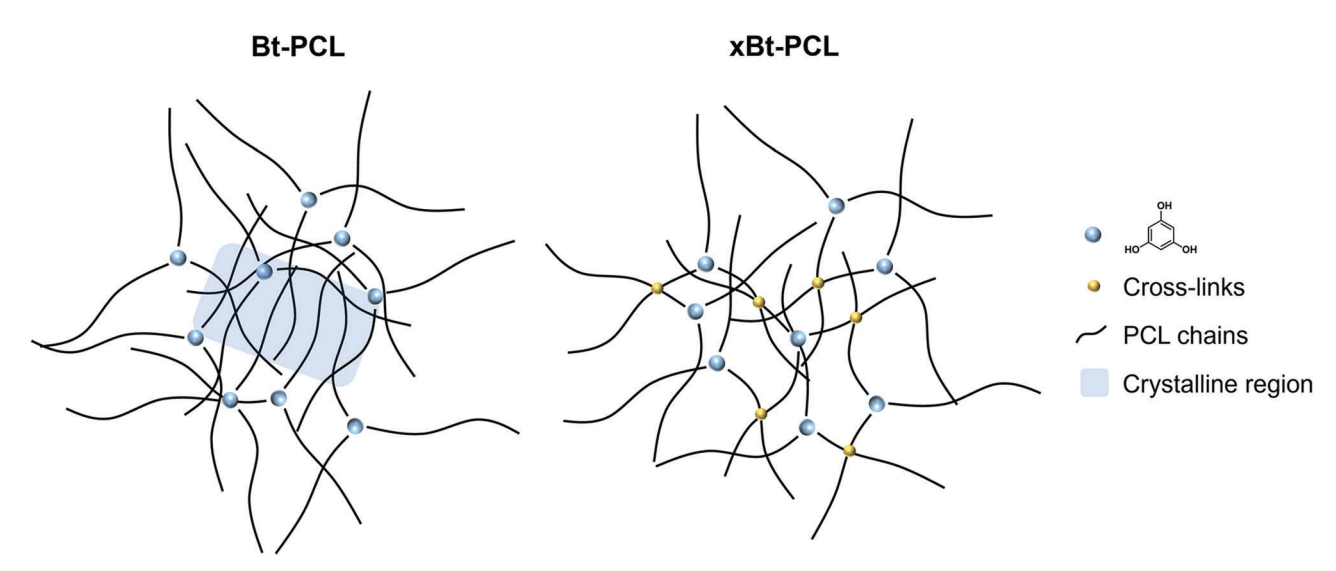
SPE composition	Ionic conductivity [S cm ⁻¹]/ temp.	Li-ion transference number	Limiting current density/temp.	Plating/stripping: overvoltage/duration time/current density	Young's modulus/temp.	Cell/mass loading/cycles/C- rate/capacity retention/operating temp./ cutoff [V]	Ref.
PCL/LiClO ₄	$1.2 \times 10^{-6}/RT$	_	_	_	_	LiNiCoO ₂ Li / – /50th/ – /65.9%/4.2 V	[24]
PCL with LATP powders/ LiClO ₄	3.6×10^{-5} /55 °C	0.58	_	150 mV/300 h/0.12 mA cm ⁻²	5.3 MPa/ -	NMC523 Li /-/20th/0.2C /70.8%/ 55 °C/4.3 V	[25]
Comb-like PCL with halloysite nanotubes/LiFSI ^{a)}	$2.7 \times 10^{-4} / 60 ^{\circ}\text{C}$	0.55	_	150 mV/1500 h/0.1 mA cm ⁻²	_	LFMP Li/1.5 mg cm ⁻² / 250th/0.2C /83.7%/ 60 °C/4.25 V (rather unstable performance)	[26]
Comb-like PCL /LiFSI	$2.5 \times 10^{-4} / 60 ^{\circ}\text{C}$	0.41	_	100 mV/800 h/0.1 mA cm ⁻²	_	LFMP Li/1.5 mg cm ⁻² /75th / 0.2C/68%/ 60 °C/4.25 V	[26]
Cross-linked star-PCL/LiTFSI ^{b)}	5.0 × 10 ⁻⁵ /60 °C 1.3 × 10 ⁻⁵ /40 °C	0.59	0.87 mA cm ⁻² / 60 °C	40 mV/1000 h/0.1 mA cm ⁻²	≈0.1 MPa/60 °C	NMC622 Li /2.5 mg cm ⁻² / 300th/1C/ 69.4%/60 °C /4.3 V NMC622 Li /2.5 mg cm ⁻² /300th/1C/ no obvious fading/ 40 °C/4.3 V	This work
Cross-linked PEO /LiBF ₄ & LiTFSI	$1.4 \times 10^{-5} / 60 ^{\circ}\text{C}$	0.23	_	_	_	NMC111 ^{c)} Li /2.4 mg cm ⁻² /15th/ 0.1C/79.3% /60 °C/4.4 V	[29]
Cross-linked PEO /LiTFSI	$1.2 \times 10^{-4}/$ 60 °C	0.32	_	45 mV/900 h /0.01 mA cm ⁻²	_	LFMP Li/ – / 100th/0.1C /87%/60 °C /4.25 V	[30]
Cross-linked PEO/PPO ^{d)} / LiTFSI /EO/PO block plasticizer	$1.3 \times 10^{-3} / 60 ^{\circ}\text{C}$	_	_	_	_	NMC622 Li / - /100th/ 0.3C /90%/ 60 °C/4.2 V	[31]

 $[\]overline{a}$ Lithium bis (fluorosulfonyl) imide; b) Lithium bis (trifluoromethanesulfonyl) imide; c) LiNi_{0.3} Mn_{0.3} Co_{0.3} O₂; d) Poly (propylene oxide).

Similar to PEO, PCL exhibits a low glass transition temperature ($T_g = -60$ °C) and mobile polymer chains to boost Liion transport, yet the coordination among carbonyl moieties and Li-ions is much weaker compared to ether-Li-ion interactions in PEO, in this way facilitating better Li-ion mobility and higher t_{\perp} . [22] Based on high degrees of crystallinity, PCL may suffer from unfavorable thermal properties (as reflected by a melting point of 60 °C that even decreases to 40-50 °C upon mixing with lithium salts) and restricted mechanical stability at higher temperatures, thereby increasing its vulnerability to lithium dendrite penetration.[13,23] While previous work introduced PCL-based SPEs, little work considered pristine PCL-SPEs for operation against high-voltage cathode materials (see Table 1).[23-25] Fonseca et al. have pioneered LiNiCoO2|PCL|Li cells with 10% LiClO₄ (lasting up to 50 cycles) for which poor Coulombic efficiency was demonstrated, while the specific capacity decaved drastically upon cycling. [24] Efforts to decrease the crystallinity of PCL included an introduction of inorganic fillers, such as halloysite, Li_{1.4}Al_{0.4}Ti_{1.6}(PO₄)₃ (LATP), also improving the achievable overall ionic conductivity, affording excellent electrochemical performance of LFP|PCL|Li cells at 60 °C and Crates of up to 1C.[25,26] Nevertheless, disadvantageous Coulombic efficiency and capacity retention were observed in case of PCLs operated in LiFe_{0.6}Mn_{0.4}PO₄ (LFMP)/LiNi_{0.5}Mn_{0.2}Co_{0.3}O₂ (NMC523) cathode-based cell configurations. Cross-linked polymer electrolytes could provide network structures that not only enhance mechanical strength but also limit the crystallinity of the electrolyte membranes. [13,27] Notably, cross-linked PCL performs faster hydrolytic degradation than pristine PCL, likely reflecting faster penetration of water into the reinforced polymer matrix. [28] Such approach has been reported to form free-standing membranes, while affording higher overall ionic conductivities for PEO-based SPEs, rendering them suitable for operation against high-voltage cathodes (see Table 1). [28–30]. [29–31] Yet, it is essential to strike a balance between mechanical properties and ionic conductivity, where end-group cross-linking may readily lead to brittleness and low elasticity of the membranes in cases where plasticizer are absent. [27]

In this contribution, a cross-linked star-shaped SPE based on PCL (denoted as xBt-PCL) is introduced that allows straightforward all-solvent-free synthesis and membrane processing, as well as robust cycling in LiNi_{0.6}Mn_{0.2}Co_{0.2}O₂ (NMC622)||Li cells, thereby providing decent specific capacity and long cycle life at higher C-rates (1C). The plain polymer structures require less synthesis efforts, reflecting lower carbon footprints in comparison to other more complex polymer matrices (e.g., single-ion conductors). Indeed, to the best of our knowledge, xBt-PCL-based SPEs demonstrate superior cycling stability among all other PCL-based and cross-linked PEO-based SPEs reported so far for exploitation in all-solid-state high-voltage

1521397, 2022, 20, Downdoaded from https://oinineithrary.wiey.com/doi/10.1002marc.202200335 by Forschungsenrum Jülich GmbH Research Center, Wiley Offine Library on (04/11/2021). Settle Terms and Conditions (https://oinineithrary.wiey.com/ems-and-conditions) on Wiley Offine Library for rules of use; OA articles are governed by the applicable Creative Commons Licensen and Conditions (https://oinineithrary.wiey.com/ems-and-conditions) on Wiley Online Library for rules of use; OA articles are governed by the applicable Creative Commons Licensen and Conditions (https://oinineithrary.wiey.com/ems-and-conditions) on Wiley Online Library for rules of use; OA articles are governed by the applicable Creative Commons Licensen and Conditions (https://oinineithrary.wiey.com/ems-and-conditions) on Wiley Online Library for rules of use; OA articles are governed by the applicable Creative Commons Licensen and Conditions (https://oinineithrary.wiey.com/ems-and-conditions) on Wiley Online Library for rules of use; OA articles are governed by the applicable Creative Commons Licensen and Conditions (https://oinineithrary.wiey.com/ems-and-conditions) on Wiley Online Library for rules of use; OA articles are governed by the applicable Creative Commons Licensen and Conditions (https://oinineithrary.wiey.com/ems-and-conditions) on Wiley Online Library for rules of use; OA articles are governed by the applicable Creative Commons Licensen and Conditions (https://oinineithrary.wiey.com/ems-and-conditions) on the applicable Creative Commons Licensen and Conditions (https://oinineithrary.wiey.com/ems-and-conditions) on the applicable Creative Commons Licensen and Conditions (https://oinineithrary.wiey.com/ems-and-conditions) on the applicable Creative Commons Licensen and Conditions (https://oinineithrary.wiey.com/ems-and-conditions) on the applicable Creative Commons Licensen and Conditions (https://oinineithrary.wiey.com/ems-and-conditions) on the applicable Creative Commons Licensen and Conditions (https://oinineithrary.wiey.com/ems-and



Scheme 1. Schematic synthesis route for preparation of Bt-PCL & xBt-PCL solid polymer electrolytes and their proposed structures. ϵ -Caprolactone was initiated by initiator (phloroglucinol), where the ring-opening polymerization (ROP) was catalyzed by tin(II) 2-ethylhexanoate. The resulting star polymers were dry-mixed with LiTFSI (and photoinitiator, benzophenone, in case of xBt-PCL), and then hot-pressed to form free-standing membranes (xBt-PCL: radiated by UV-light).

cells, also considering other salient features comprising, e.g., limiting current density, Young's modulus of the all-dry polymer membranes and higher C-rate applicability (Table 1). Indeed, the outstanding cycling performance is mainly attributed to the cross-linked structures that enable more homogeneous lithium metal deposition and better interfacial properties, as successfully demonstrated by combining scanning electron microscopy (SEM) and ⁷Li solid-state NMR analysis.

2. Results and Discussion

2.1. Polymer Membrane Properties

The synthesis route for producing star-shaped PCL and the membrane processing are highlighted in **Scheme 1**. Since the initiator phloroglucinol can be well dissolved within liquid ϵ -caprolactone monomers, bulk polymerization was conducted. Notably, even for membrane processing, all the components were dry-mixed and hot-pressed without solvents involved, thereby excluding the presence of residual solvents that eventually result in overrated ionic conductivity (e.g., in case of solvent-casting). This in principle yields a "green" SPE without prior contact to any hazardous organic solvents; after cross-linking, translucent, elastic,

and self-standing polymer membranes were obtained (Figure S1, Supporting Information).

The corresponding Li-ion concentration was varied to optimize the overall ionic conductivity of the polymer electrolytes, as shown in Figure 1 (left), where Bt-PCLs with different LiTFSI contents, ranging from [C=O]:[Li] ratios of 7:1–3:1 were prepared. At low contents of lithium salt, an abrupt increase of ionic conductivity is observed at higher temperatures (that is, above the melting point), reflecting the semicrystalline nature of PCL. Consequently, trends of ionic conductivity gradually display Vogel-Fulcher-Tammann (VFT) behavior with increasing salt contents, illustrating that the lithium salt indeed has a plasticizing effect on the considered polymers (limiting crystalline phases), thereby increasing the achievable ionic conductivity in the lower temperature region.[33] Upon further addition of LiTFSI, i.e., conditions of over-saturated lithium salt ([C=O]:[Li] = 4:1, 3:1) tend to inhibit the dissociation of Li-ions, yielding lesser fractions of mobile "free" charge carriers and accordingly reduced ionic conductivity. [34,35] Bt-PCL yielded the highest ionic conductivity at a [C=O]/[Li] ratio of 5:1 (reflecting a Li-ion concentration of 1.58 mol L⁻¹), both at 40 and 60 °C. Different compositions were also employed for cross-linked polymer electrolytes xBt-PCL (see Figure S2, Supporting Information), yet, optimal ionic conductivities were obtained at a [C=O]/[Li] ratio of 5:1 as well,

15213927, 2022, 20, Downloaded from https://onlinelibrary.wiley.com/doi/10.1002/marc.202200335 by Forschungszentrum Jülich GmbH Research Center, Wiley Online Library on [04/11/2022]. See the Terms and Conditions

conditions) on Wiley Online Library for rules of use; OA articles are governed by the applicable Creative Commons License

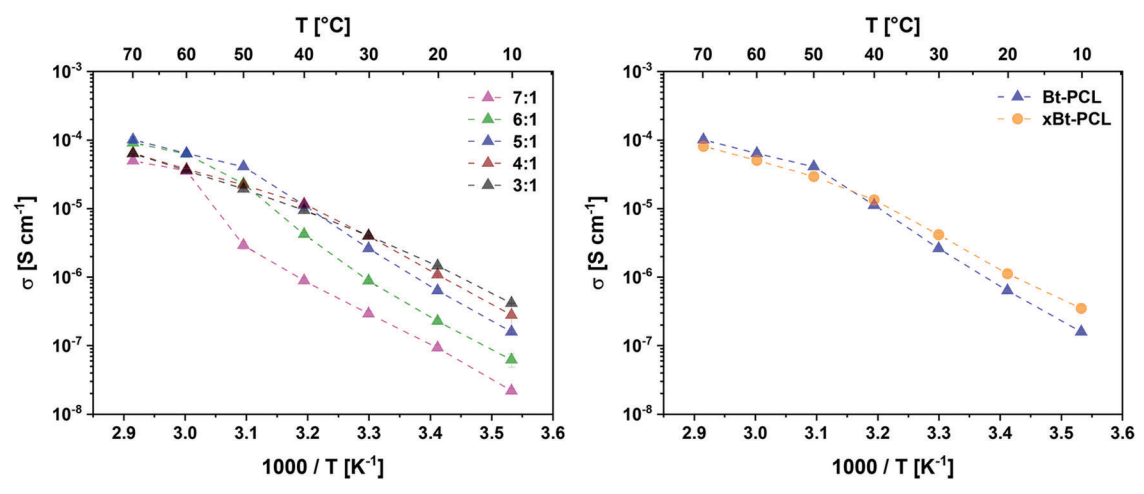


Figure 1. Temperature-dependent overall ionic conductivity of Bt-PCL with different LiTFSI contents ([C=O]:[Li]) (left); comparison of Bt-PCL and xBt-PCL at [C=O]:[Li] = 5:1 (right).

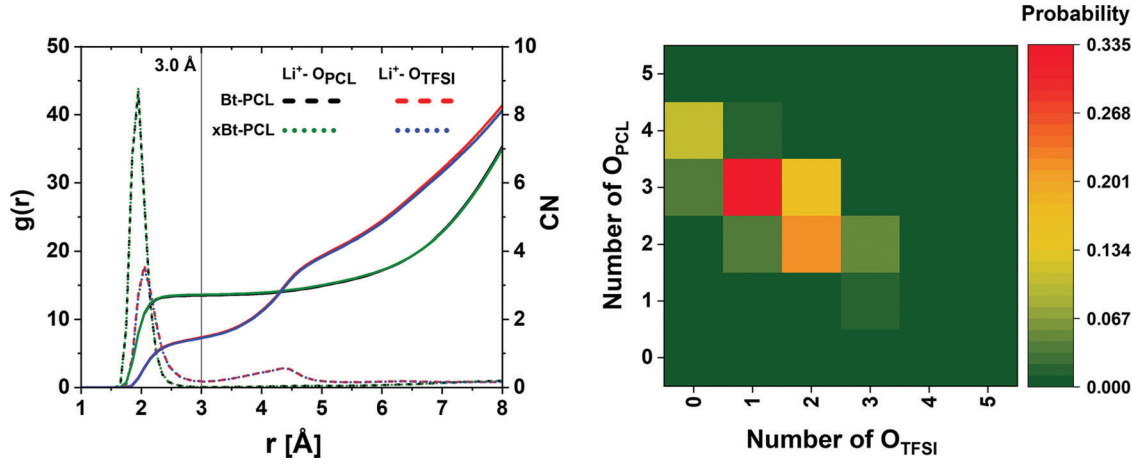


Figure 2. Radial distribution functions (dash lines, left y-axis) and corresponding coordination number (CN, solid lines, right y-axis) between Li-ion and oxygen atoms of PCL arms and TFSI anion in Bt-PCL and xBt-PCL systems at 400 K. Vertical line defines the first coordination shell (left). Probability distribution of finding $n \, O_{PCL} + m \, O_{TFSI}$ combination of oxygen atoms within the first coordination shell of Li⁺ (right).

yielding values of 1.3×10^{-5} S cm⁻¹ (40 °C) and 5×10^{-5} S cm⁻¹ (60 °C) (Figure 1, right). Note that the more amorphous phase in xBt-PCL enables much better thermal stability and enhanced mechanical properties compared to pristine Bt-PCL, emphasizing that the formation of cross-linked junctions effectively hinders or fully inhibits polymer chain folding and reorganization during crystallization, as shown by differential scanning calorimetry (DSC) analysis (Figure S3, Supporting Information). [28] During second heating, a corresponding glass transition temperature (T_{o}) , crystallinity temperature (T_{c}) , and melting temperature (T_{m}) are noticed in case of Bt-PCL, while T_c and T_m are barely visible for xBt-PCL. Yet, it still possesses certain degree of crystallinity which can be also seen at the slight bending point at 50 °C in the ionic conductivity measurements. Even though a phase transition appears, key features of the introduced SPEs such as the electrochemical performance are demonstrated purposely at 60 °C, which is above the threshold, highlighting better mechanical properties of xBt-PCL. An increase in $T_{\rm g}$ from -45.9 to -38.8 °C

indicates that the cross-linked structures slightly impair polymer chain flexibility as well as ion transport capability, consistent with obtained ionic conductivity data at higher operation temperatures where the molecular chains are in disordered arrangements.

Structural and dynamic correlations governing the Li-ion (Li+) transport through the polymer electrolyte membranes were derived from atomistic molecular dynamics (MD) simulations, initially analyzing local environments of Li⁺. Figure 2a shows the radial distribution functions (g(r)) of oxygen atoms of both PCL and TFSI- around the cations, where a strong preference of Li+ to be coordinated by oxygen atoms is clearly illustrated by large first peaks in g(r) and corresponding coordination numbers (CN). The first Li⁺ coordination shell can be defined as position of the first minimum in the corresponding g(r), shown as vertical line at r =3.0 Å. In the Bt-PCL and xBt-PCL systems, the Li+ first coordination shell environment is dominated by PCL oxygen atoms (on average 2.7 O_{PCL}), while TFSI oxygen atoms are about half of that (on average 1.44 O_{TESI}). Note that there is almost no difference

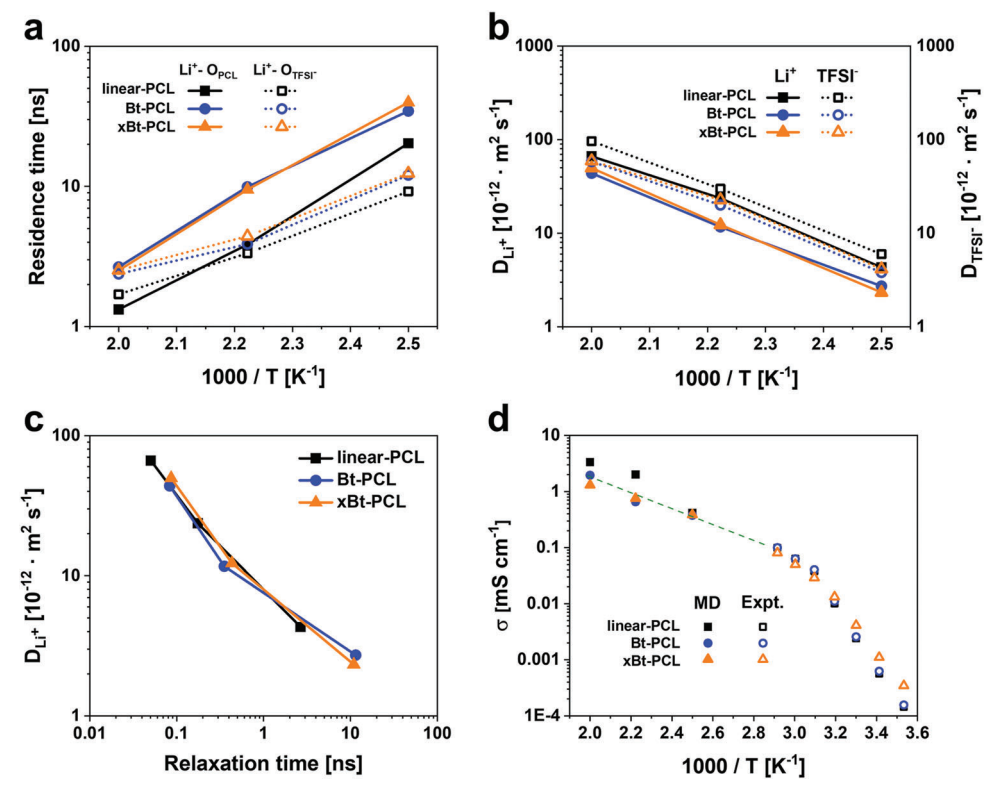


Figure 3. Dynamic correlations obtained from MD simulations for linear-PCL, Bt-PCL, and xBt-PCL with 5:1 ratio of polymer groups and cations: a) Temperature dependence of residence times of neighboring O atoms near Li⁺. B) Self-diffusion coefficients of cation and anion as a function of temperature. C) Li⁺ diffusion versus relaxation time of polymer segments in the matrix. D) Ionic conductivity obtained from MD simulations at higher *T* and compared to lower *T* range conductivities reported from experiments.

between Bt-PCL and xBt-PCL local environments of Li⁺, clearly indicating that the cross-linking does not affect the coordination of cations. Figure 2 shows the distribution of local environments, with the most probable one comprising 3 $O_{PCL}+1$ O_{TFSI} composition, though 2 $O_{PCL}+2$ O_{TFSI} coordination also shows significant probability. Yet, there are very minor effects of cross-linking on the distribution of the Li⁺ environments.

Figure 3 compares dynamic properties and correlations obtained from MD simulations as a function of temperature for linear-PCL, Bt-PCL, and xBt-PCL systems, whereas Figure 3a exhibits residence times of oxygen atoms in the first coordination shell of Li+. As anticipated, the fastest exchange of polymer atoms near the cations occurs in the linear-PCL system. Upon transition to Bt-PCL or xBt-PCL, the residence times of polymer oxygen atoms rise significantly (factor of 2-3), while the residence time of TFSI oxygens near Li+ only increases slightly. Note, while the cross-linking in xBt-PCL system restrains polymer chain dynamics on the length scale comparable to the chain radius of gyration, the ability of Li⁺ to change its local environment, i.e., move from one set of oxygen atoms to another, is not affected. It also worth pointing out that as temperature decreases the residence time of O_{PCL} near Li^+ becomes noticeably longer than the residence times of O_{TFSI}. Figure 3b displays the temperature dependence of cation and anion self-diffusion coefficients in the investigated systems. Considering the longer residence time of Li⁺ with oxygen atoms from polymer, it is not surprising that the TFSI anion has a higher self-diffusion coefficient (D) compared to Li⁺. A strong correlation of $D_{\rm Li+}$ with polymer segmental motions is readily illustrated in Figure 3c where $D_{\rm Li+}$ is plotted versus the corresponding structural relaxation time defined as dynamic structure factor (S(q,t)) for O_{PCL} atoms for q=1.0 Å⁻¹. In all systems, a strong coupling between polymer local motions and Li⁺ diffusion is evident. Note that all MD simulations were conducted well above the glass transition temperature, as at lower temperatures, Li⁺ motion can become decorrelated from polymer dynamics.^[36]

Figure 3d shows the ionic conductivity obtained from MD simulations at higher temperatures and extrapolated for comparison with experimental data at lower temperatures. Notably, the temperature dependence of ionic conductivities for both Bt-PCL and xBt-PCL materials obtained from MD simulations is in excellent agreement with experimental data. Contributions to the ionic conductivity also allow to calculate the so-called degree of ion dissociation (α), defined as the ratio of "real" conductivity derived when including all the dynamic ion-ion correlations and the ideal conductivity obtained based on the Nernst-Einstein approach exploiting self-diffusion coefficients. In all systems α is around 0.45–0.55, while the Li-ion transference numbers (t_{\perp}) amount to ≈0.55 under anion-blocking conditions. These characteristics indicate a significant decoupling between anion and cation motion. The experimentally obtained t_{\perp} values based on application of the Bruce-Vincent method are 0.46 ± 0.05 and 0.59 ± 0.05 in case of Bt-PCL and xBt-PCL (potentiostatic polarization experiments and impedance data are included in Figure S4, Supporting In-



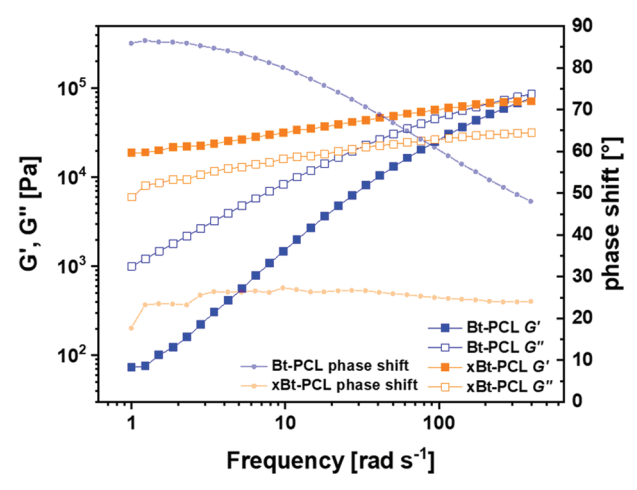


Figure 4. Storage (G'), loss moduli (G''), and phase shift versus frequency at 60 °C for the materials Bt- and xBt-PCL.

formation). Since the ion-ion interactions are not negligible in nonideal electrolytes, these numbers were suggested to be referred to as a limiting current fraction F_{\perp} (see Bruce and Gray).^[37] Despite that, Rosenwinkel et al. have shown a model-free approach to determine t_{\perp} values directly from the electrophoretic mobilities μ of the ionic species by electrophoretic NMR (E-NMR) of salt-in-polymer electrolytes that agrees well with literature data obtained via the Bruce-Vincent method.[38] The difference of t_{\perp} between Bt-PCL and xBt-PCL was tentatively attributed to restrained mobility of anions within the cross-linked network, yet contradicting the results of MD simulations; this renders the assignment somewhat ambiguous.^[39] Another possibility might be potential effects of directional correlations between different anions, which however were not further investigated. Nonetheless, the experimental t_{\perp} values in view of the error margins are in reasonable agreement with the results of the MD simulations, and the impact of the higher t_{\perp} for xBt-PCL is well reflected by the electrochemical performance of the respective cells.

In Figure 4, the rheological properties of the PCL-based materials are displayed at a temperature of 60 °C (both noncross-linked and cross-linked), where the storage modulus (G') represents the material's ability to store energy elastically, whereas the loss modulus (G") is related to the amount of energy scattered within the considered materials, i.e., viscous parts of the samples. The PCLbased SPEs can be considered mainly as elastic solids when G'is higher than G'', like in case of xBt-PCL ($G' \approx 0.1$ MPa at high frequency), that is, the phase shift (phase angle between vector contributions $G^* = G' + G''$ and G') is below 45°, maintaining values between 20° and 30°. [40] For Bt-PCL, G' is lower than G" even at very high frequencies and the phase shift approaches 90° at low frequencies, reflecting primarily a viscous behavior due to melt of polymer at 60 °C. This observation corroborates the beneficial impact of cross-linking on both mechanical and thermal stability, which are critical entities that enable long-term suppression of lithium dendrite growth upon cell cycling. Despite a threshold value of G' > 6 GPa introduced by Monroe and Newman considered relevant for complete mechanical suppression of Li dendrites, simulations of PEO indicate the feasibility of homogeneous Li deposition even in cases of G' > 1 MPa.^[23,41] In addition, cross-linked PEO systems with lower modulus (0.1 MPa) may also sufficiently suppress inhomogeneous Li deposition, in good agreement with the data for PCL-based electrolytes, which are at the same order of magnitude.^[42] Nonetheless, moduli are not the only relevant factor to be considered, as demonstrated in the present case, where rheologic properties appear as predominant factor that mitigate Li dendrite formation.^[43]

2.2. Lithium Dendrite Reduction and Suppression

C-rate analysis was conducted for both NMC622|Bt-PCL|Li and NMC622|xBt-PCL|Li cells to determine the likely impact of crosslinked polymer electrolytes on the cycling performance, particularly at reasonably high current densities (> 1C, 0.45 mA cm⁻²), where inhomogeneous Li deposition and Li dendrite growth is anticipated according to Sand's model. [44,45] In Figure 5a, the charging profile for Bt-PCL-based cells fluctuates slightly starting from 0.1C (blue line); the deviation becomes much more pronounced with increasing current densities (e.g., at 1C, brown line), resulting in overestimated specific charge capacities while maintaining reasonable specific discharge capacities, associated with decreased Coulombic efficiencies.^[18] In contrast, cell failure does not occur for xBt-PCL-based cells even at rates of up to 2C (Figure 5b; and Figure S5, Supporting Information). Note that from the literature, the so-called "voltage noise" is tentatively attributed to abundant microshort circuits induced by HSAL deposits after considering different aspects of PEO-based SPEs, including the membrane thickness, oxidative stability, or mechanical strength.[17,18] PCL-based SPEs are oxidatively stable even at potentials above 5 V versus Li|Li+ (Figure S6, Supporting Information), so that any contributions from polymer oxidation or decomposition are initially excluded as origin of the observable "voltage noise." Rather, direct evidence that correlates "voltage noise" and cell failure to the presence of dendritic/"mossy" Li deposits is provided, particularly distinguishing the actual morphology of Li deposits based on ⁷Li solid state NMR data (characteristic ⁷Li NMR signals at chemical shifts of 240–250 ppm reflect contributions from "smooth" bulk lithium, whereas "mossy"/dendritic lithium fractions exhibit peaks centered at 260/270 ppm, respectively). [1,46,47] NMC622|SPE|Li cells were first cycled at 1C (60 °C) for 50 cycles (see Figure S7, Supporting Information) prior to the ⁷Li NMR measurements. Unlike the cells operated with Bt-PCL, where rather unstable and low Coulombic efficiencies are observed (e.g., due to severe extra charge capacities caused by "voltage noise"), the electrochemical performance of xBt-PCL-based cells remains steady, comparable to the C-rate tests. All the cycled cells were disassembled in a dry room, with 6 mm samples punched out (yielding a sandwich including lithium metal, SPE and NMC cathode) and subsequently placed into pouch-type housings, thereby yielding thinfilm cells suitable for ⁷Li NMR analysis. In Figure 5c, in case of Bt-PCL, the ⁷Li NMR spectrum displays two peaks, one centered at ≈245 ppm (bulk Li) and a broader peak at 260–270 ppm consisting of "mossy"/dendritic Li deposits. Note that more inhomogeneous ("rougher") surface morphologies of Li deposits tend to shift the respective ⁷Li NMR peak to higher ppm values (due to,

15213927, 2022, 20, Downloaded from https://onlinelibrary.wiley.com/doi/10.1002/marc.202200335 by Forschung

entrum Jülich GmbH Research Center, Wiley Online Library on [04/11/2022]. See the Terms and Conditions (https://onlinelibrary.wiley

conditions) on Wiley Online Library for rules of use; OA articles are governed by the applicable Creative Commons License

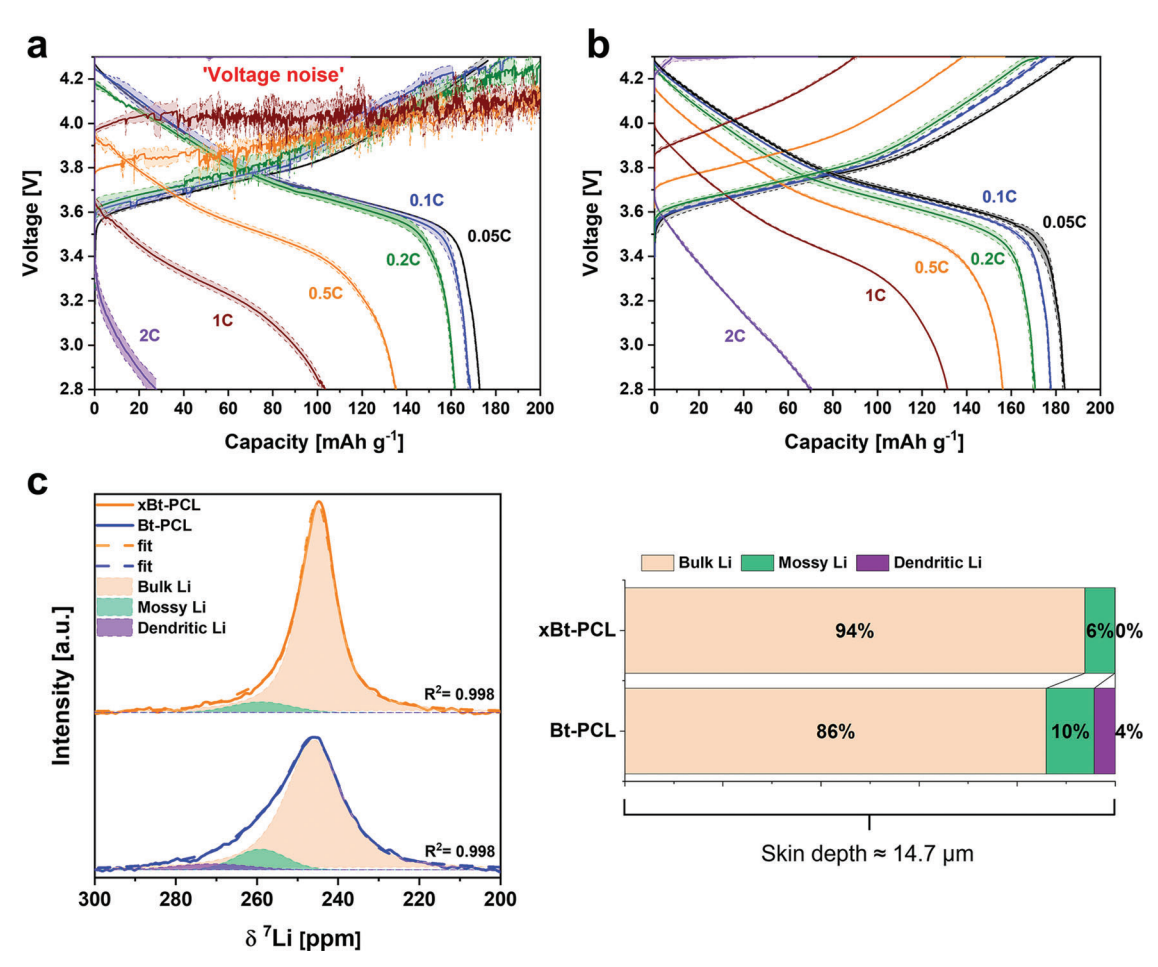


Figure 5. Charge/discharge profiles (with error margins) of NMC622|SPE|Li cells operating with a) Bt-PCL and b) xBt-PCL-based SPEs at different C-rates and 60 °C. Note that the "voltage noise" was not intentionally created, where all cells were prepared with same procedures and setup. c) 7 Li solid-state NMR spectrum of NMC622|SPE|Li cells after 50 cycles of plating and stripping with fitting result (R^{2} stands for the coefficient of determination), as well as peak composition from spectral fitting; note that the bulk lithium was only fractionally detected due to the skin depth effects.

e.g., the anisotropy of magnetic susceptibility, paramagnetic, and orientational effects). $\sp(47)$

The deconvolution of the corresponding spectra was done with line-shape fitting (Voigt function) via a customized MATLAB script based on peakfit.m, where distinct peak areas centered at \approx 260 and 270 ppm were obtained (10% and 4% integral fractions in case of Bt-PCL) representing mossy and dendritic Li deposits that likely are connected to the occurring "voltage noise." [48] In contrast, negligible amounts of dendritic Li and lesser fraction of "mossy" Li (suppressed by the robust membrane) were derived for the cells operating with xBt-PCL. Note that due to the so-called skin depth effects (14.7 µm at a magnetic field of 4.7 T), the penetration of radio-frequency fields is limited, rendering the overall reservoir of the rather thick Li metal anode (300 µm) not fully detectable, whereas contributions from Li microstructures deposited on top of bulk Li surfaces are entirely captured based on relatively low amounts of Li deposits compared to previously reported data, i.e., 0.45 mAh cm⁻² compared to 2.14 mAh cm⁻², which reflects a Li deposit thickness of 11–12 $\mu m.^{[46,49]}$

Consequently, higher amounts of inhomogeneous Li deposits occurred in cells with Bt-PCL, as monitored based on ⁷Li NMR, in agreement with the observed "voltage noise." Indeed, the well-

established method is capable of directly verifying the presence of inhomogeneous deposits based on the characteristic chemical shifts of the individual Li metal species, indicating nearly no dendritic Li morphology and less mossy Li for xBt-PCL-based cells. Single-side Li deposition experiments were performed to validate the anticipated ability of Li dendrite suppression when operating cells with the cross-linked PCL-based SPEs. Therefore, a current density of 0.1 mA cm $^{-2}$ was applied to Li|SPE|Li cells at 60 °C (with cut-off voltage: 1.5 V; Figure S8, Supporting Information), exhibiting an overvoltage on the order of \pm 40 mV upon Li plating/stripping. After up to 92 and 105 h in case of Bt-PCL- and xBt-PCL-based cells, polarization eventually appears due to neardepletion of Li species at the working electrode surfaces, where a localized space charge associated with a large electric field is created that initiates Li dendrite growth, according to Chazalviel's model.^[50] The Bt-PCL-based cells short-circuit immediately upon voltage increase while in case of xBt-PCL, the cells display serious polarization until the cut-off voltage rather than complete failure, demonstrating better mechanical properties to avoid shortcircuit. These cells were disassembled in an Ar-filled glovebox for postmortem SEM analysis. As the polymer electrolytes were highly adhesive to the Li metal surfaces, it was not possible to

15213927, 2022, 20, Downloaded from https://onlinelibrary.wiley.com/doi/10.1002/marc.202200335 by Forschungszentrum Jülich GmbH Research Center, Wiley Online Library on [04/11/2022]. See the Terms

conditions) on Wiley Online Library for rules of use; OA articles are governed by the applicable Creative Commons License

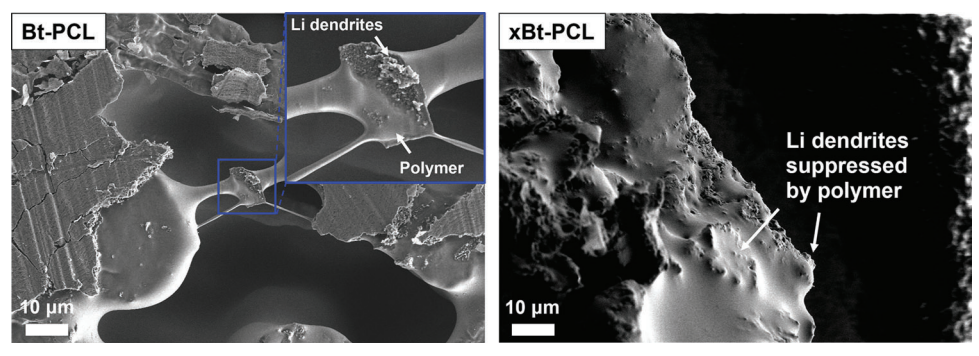


Figure 6. SEM images of Bt-PCL-based cells after plating for 114 h until short-circuit and xBt-PCL-based cells after plating for 117 h. Note that the white dots on the right side of the right figure may refer to the sample holder.

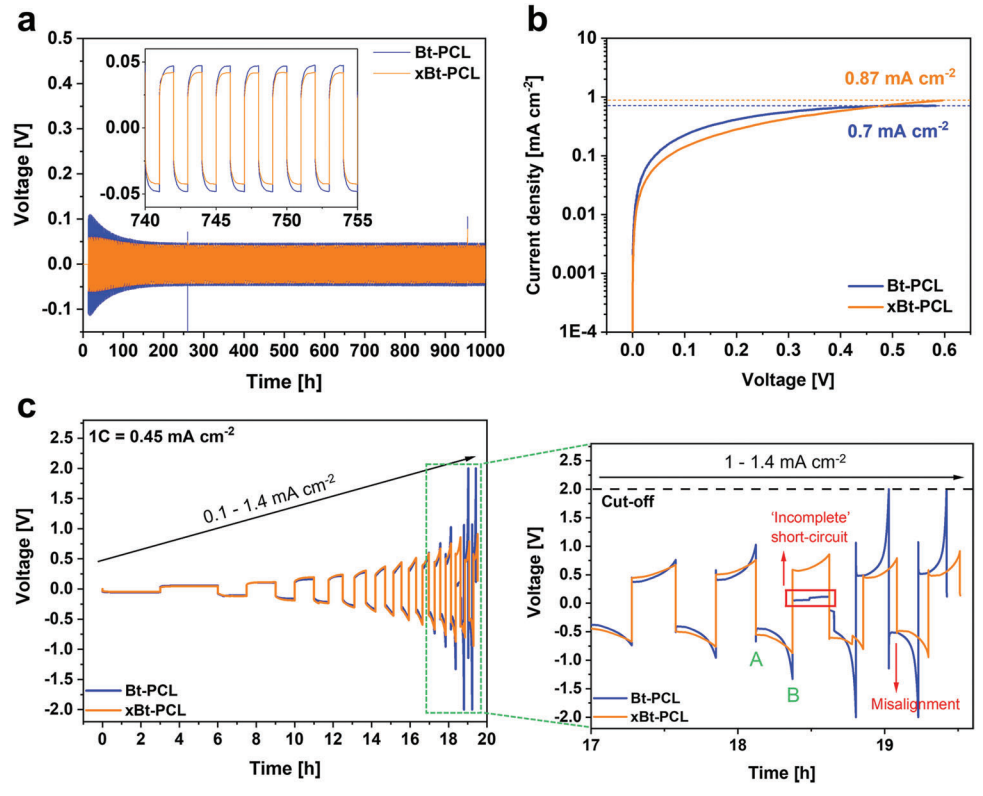


Figure 7. a) Long-term lithium plating/stripping processes at a current density of 0.1 mA cm⁻², b) limiting current density, and c) C-rate analysis, ranging from 0.1 to 1.4 mA cm⁻², operating Li|SPE|Li symmetric cells at 60 °C.

fully separate them, therefore in **Figure 6**, the cracked (Bt-PCL) or edged parts (xBt-PCL) of sandwiched samples were observed with counter electrodes facing up (toward the direction where Li deposited).

Indeed, the accumulated dendritic lithium penetrating through the Bt-PCL membrane is clearly visible, whereas xBt-PCL is capable of suppressing inhomogeneous Li deposits effectively, even at fairly large amounts of 3 mg cm⁻² of plated lithium (compared to single-ion conductor symmetric cells that short-circuited upon 1.1 mg cm⁻² of Li plated at similar conditions: current density of 0.1 mA cm⁻² and 60 °C).^[51] Two SPEs were compared at extreme conditions, and the obtained results emphasize that cross-linked polymer electrolytes unam-

biguously enable a reasonable restraint of Li dendrite owing to their superior mechanical and thermal properties, consistent with the ⁷Li NMR data, reflecting that xBt-PCL-based electrolytes are capable of avoiding "voltage noise" thus facilitating better cell performance.

In a long-term lithium plating/stripping experiment, no significant differences of the overvoltage could be identified for Bt-PCL and xBt-PCL-based cells operating at low current density (0.1 mA cm⁻²; **Figure 7**a). Bt-PCL-based cells possess an initially higher overvoltage of 110 mV that later stabilizes at 45 mV. Both Li|SPE|Li cells are operational for up to 1000 h without cell failure. Note that the arcing behavior of both overvoltage profiles is attributed to concentration polarization effects, yet milder in



- Acrolocular
Rapid Communications
www.mrc-journal.de

case of xBt-PCL-based cells, likely due to the higher t_{+} (lesser anion concentration gradients). [51] To determine the potential of fast charging in case of Li|SPE|Li cells, a C-rate test (Figure 7c) was performed, applying current densities ranging from 0.1 to 1.4 mA cm⁻² (1C \approx 0.45 mA cm⁻²), in each case achieving comparable amounts of Li deposit (0.3 mAh cm⁻²). Based on Chazalviel's model, a limiting current density J* is determined as a crossover value of high and low current-density regimes, reflecting the maximum current density that can be ideally applied prior to ion depletion will occur, thereby inducing Li dendrite growth ("Sand's time"). [45] With the measured limiting current densities of 0.87 and 0.7 mA cm⁻² for xBt-PCL and Bt-PCL-based cells (Figure 7b), the corresponding overvoltage profiles of cells in the Crate test are distinguishable starting from a current density of 1 mA cm⁻², particularly at profile regions A and B, reflecting start and end of Li deposition at the working electrode or Li dissolution at the counter electrode (Figure 7c). An immediate drop in overvoltage at region A is attributed to a kinetic hindrance of Li deposition (or dissolution) beneath the electrode surface films, i.e., due to limitations of Li-ion transport through the electrode|electrolyte interfaces.^[52] "Fresh" Li settled onto previous deposits of "roughened" lithium surfaces results in decreased overvoltage, followed by a gradual increase in the event that ionic concentrations drop at the electrode surfaces.^[45] A similar trend as seen in J^* for both samples $(J^*_{xBt-PCL} > J^*_{Bt-PCL})$ is indeed observed in the C-rate test upon applying a current density of 1 mA cm⁻² and higher. For Bt-PCL-based cells, onset of Li dendrite growth occurs at a current density of 1.2 mA cm⁻², as evidenced by serious polarization induced by Li-ion depletion at region B, as well as sudden voltage drop to zero due to "incomplete" short-circuit of the respective cells upon Li plating (while the overvoltage returns to its normal range of value afterward). [53] The latter observation might be explained by the thermo-fusible effect, where Li dendrites act as fuse that burns once a sufficiently high enough current passes through it. [53,54] The misalignment of the two overvoltage profiles can be also attributed to an "incomplete" short circuit of Bt-PCL-based cells. At higher current densities (1.3 and 1.4 mA cm⁻²), polarization of the Bt-PCL-based cells becomes more severe so that the cut-off voltage of 2 V is reached, which can be related to higher rates of Li dendrites growth.^[55] In contrast, xBt-PCL-based cells exhibit no significant changes of the overvoltage at regions A and B, even at current densities of up to 1.4 mA cm⁻², likely indicating a more efficient charge transfer at the electrolyte|electrode interfaces, and more homogeneous Li deposition, in this way fostering better Li dendrite suppression, in agreement with the obtained NMR and SEM data, respectively.

2.3. Cycling Performance

The cycling stability of NMC622|SPE|Li cells is shown in **Figure 8**a,b at 40 and 60 °C, respectively. For cell formation, an initial rate of 0.05C was applied to the cells, followed by long-term cycling at a charge/discharge rate of 0.1C. The mass loading of the NMC622 electrode was 2.5 mg cm⁻² (comparatively low if targeting 300 Wh kg⁻¹ at cell-level where mass loadings > 20 mg cm⁻² would be required), yet fairly comparable and even higher than that of current all-solid-state high-voltage LMBs (Table 1).^[56] At 60°C, xBt-PCL-based cells exhibit an initial spe-

cific discharge capacity of 180 mAh g⁻¹ (theoretical capacity: 175 mAh g⁻¹) and have much better capacity retention (86% after 60 cycles) compared to Bt-PCL-based cells (72%), attributed to a higher t_{\perp} value that yields less concentration polarization and thereby lower internal resistances. This is in good agreement with the electrochemical impedance spectroscopy (EIS) spectra (Figure 8c) where the changes of the resistance of charge transfer R_{CT} prior to and after formation are distinct between the cells, whereas the resistances of solid electrolyte interface (SEI) $R_{\rm SEI}$ remain similar. The equivalent circuit model invoked for fitting of the Nyquist plots is also displayed. Note that the surface analysis of electrodes such as X-ray photoelectron spectroscopy (XPS) measurements for SEI or cathode electrolyte interface (CEI) are rather challenging, since the utilized polymer electrolytes were too adhesive to be separated from the electrodes. Another contribution to the better cycling stability of xBt-PCL-based cells comprises lesser formation of inhomogeneous or dendritic Li deposits, owing to favorable thermal and mechanical properties. In Figure 8a, xBt-PCL-based cells yield stable Coulombic efficiency (CE), while for Bt-PCL-based cells, overrated specific charge capacities likely caused by Li dendrite-induced "voltage noise," and thus arbitrary low CE are observed, comparable to observations from the ⁷Li solid-state NMR experiments. Interestingly, the Bt-PCL-based cells show a rather steady CE at lower temperature (40 °C) primarily because of enhanced mechanical stability with features of elastic solids at the high frequency range (Figure S9, Supporting Information), thereby boosting achievable cell performances. The decent cycling performance of xBt-PCL-based cells at a current density of 0.1C exhibits comparable results to those reported^[29] (Table 1), even at slightly higher cutoff voltage of 4.3 V. In addition, this is also to date the first solid-state LMB based on pristine PCL SPE that successfully operated with NMC622 cathodes at 40 °C.

To reveal the potential of PCL-based SPEs for faster charging applications, xBt-PCL based cells were cycled at higher C-rate (1C) with several steps of formation process (3 cycles of 0.05C, 0.1C, 0.2C, and then 0.5C) at both 60 and 40 °C. However, in cells with a reference NMC622 cathode, the specific discharge capacity faded rapidly (Figure 9a) at high current densities, mainly due to higher interfacial resistances that reflect charge transfer restrictions arising from contact losses at the electrolyte|electrode interfaces, especially within the porous cathode composites. [57,58] Consequently, prior to cell assembly, 1.5 wt% of PCL-based star polymer was introduced into the cathode slurry upon electrode preparation, replacing half the amount of polyvinylidene difluoride (PVdF) binder, thereby increasing the fraction of Li-ion conducting species within the composite cathode and affording better interfacial contacts.^[57] As shown in Figure 9a, despite that the initial specific discharge capacity reduced from 132 to 121 mAh g⁻¹, which may be due to larger SEI resistance, all the cells with PCL-containing cathodes enable significantly improved capacity retention, ranging from 24.9% to 69.4% after 300 cycles, compared to the reference cells. Enhanced ion transport within the active material is also reflected in the EIS spectra (Figure 9c), where $R_{\rm CT}$ (middle-frequency range) of PCL-containing cathodes is almost three times less than that of the reference NMC622 cathode after long-term cycling. Moreover, the cells were able to be cycled up to the 500th cycle without failure, though merely at 55.7% capacity retention, which so far represents a superior

15213927, 2022, 20, Downloaded from https://onlinelibrary.wiley.com/doi/10.1002/marc.202200335 by Forschungs

zentrum Jülich GmbH Research Center, Wiley Online Library on [04/11/2022]. See the Terms

ions) on Wiley Online Library for rules of use; OA articles are governed by the applicable Creative Commons License

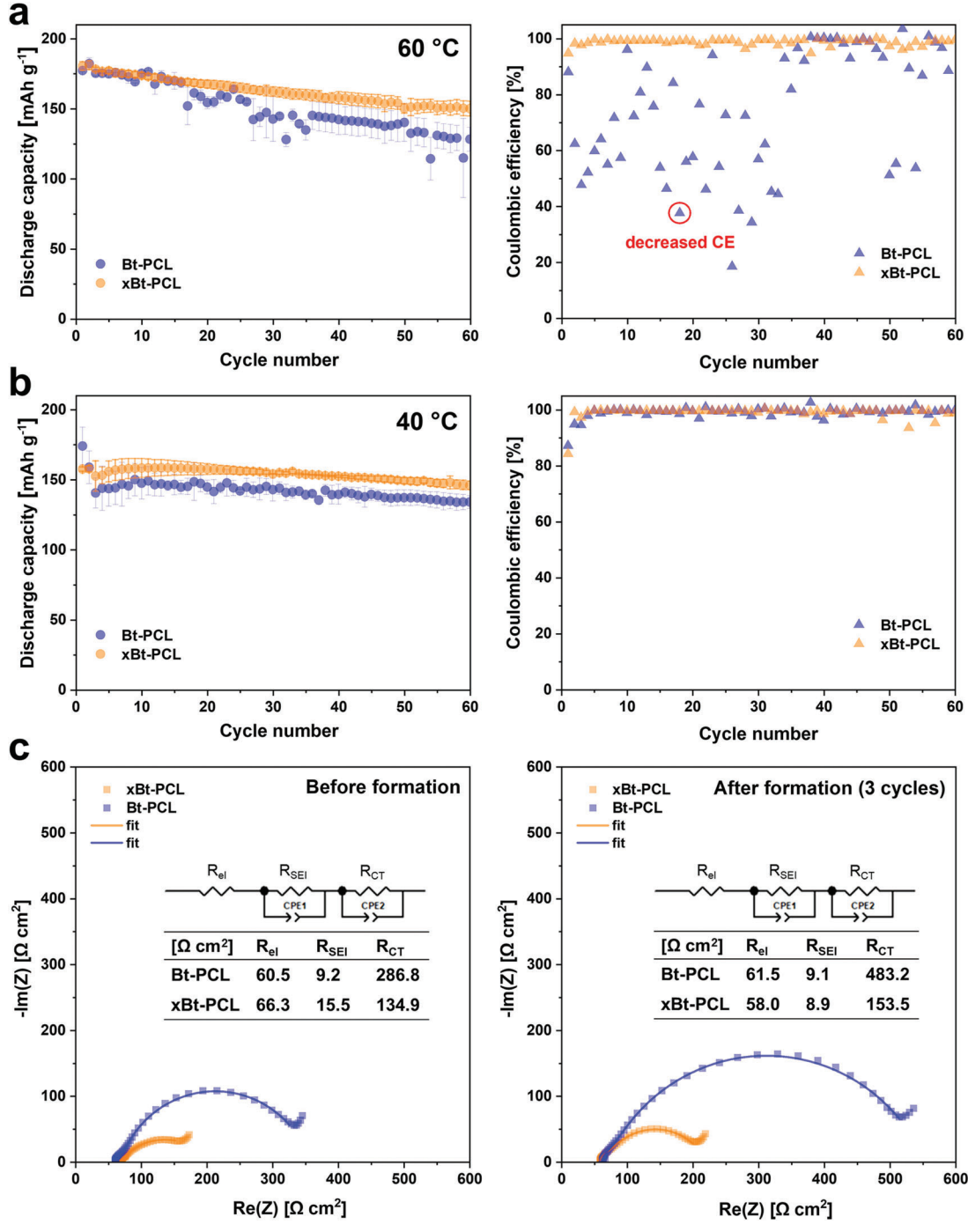


Figure 8. Cycling stability (with error margins) and Coulombic efficiency of NMC622|SPE|Li cells with Bt-PCL and xBt-PCL-based SPEs at a) 60 °C b) 40 °C (formation with 0.05C for 3 cycles, and cycling at 0.1C at 2.8–4.3 V). c) Impedance spectra, equivalent circuit model, and fitting results of NMC622|SPE|Li cells prior to and after formation at 60 °C. The impedances are normalized to areal resistances in units of Ω cm² (resistances were multiplied with a factor 0.785 from the applied electrode area).

performance among other PCL-based all-solid-state high-voltage batteries. Notably, at a temperature of 40 °C, owing to slower degradation processes, the achieved capacity retention when operating these cells is much better (Figure 9b, ref. cathode: from 24.9% to 38.3%, PCL-cathode: from 69.4% to no obvious fading). The cells with PCL-cathodes exhibit no obvious fading of specific

discharge capacity, despite the reduced initial capacity of 44 mAh g $^{-1}$. Nonetheless, the ionic conductivity of PCL-based SPEs (1.3 \times 10 $^{-5}$ S cm $^{-1}$ at 40 °C) should be further improved to enhance the exploitable specific capacity at lower temperatures, e.g., by introducing oligomers or inorganic nanofillers, or by tailoring the polymer configuration to short-chain comb-like structures,

15213927, 2022, 20, Downloaded from https://onlinelibrary.wiley.com/doi/10.1002/marc.202200335 by Forschungszentrum Jilich GmbH Research Center, Wiley Online Library on [04/11/2022]. See the Terms

ons) on Wiley Online Library for rules of use; OA articles are governed by the applicable Creative Commons License

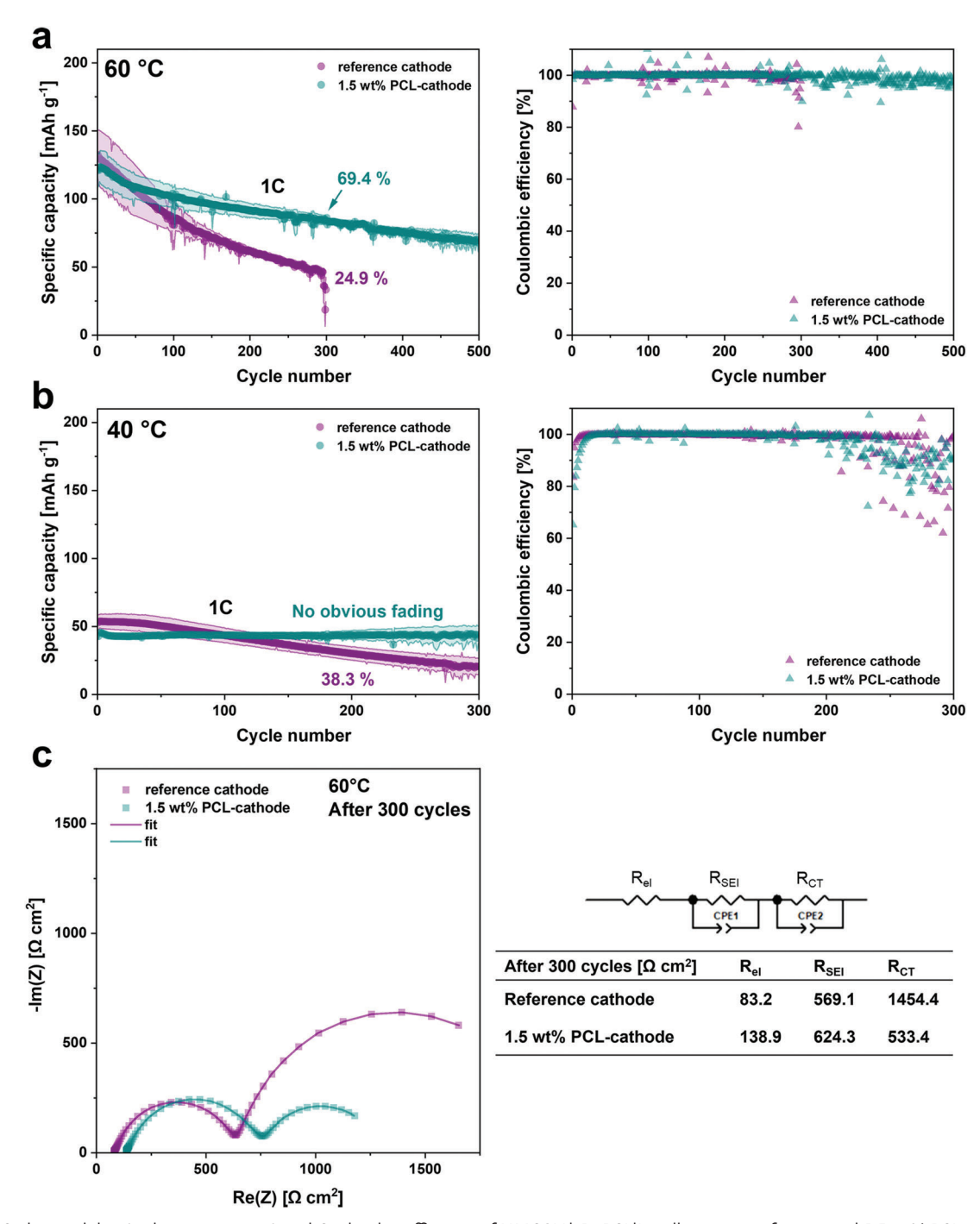


Figure 9. Cycling stability (with error margins) and Coulombic efficiency of NMC622|xBt-PCL|Li cells using a reference and 1.5 wt% PCL-cathode at a) 60 °C b) 40 °C. c) Impedance spectra, equivalent circuit model, and fitting results of NMC622|xBt-PCL|Li cells after 300 cycles at 60 °C. The impedances are normalized to areal resistances in units of Ω cm² (resistances were multiplied with a factor 0.785 from the applied electrode area).

in this way diminishing the likely presence of crystalline domains. The electrochemical performance of several all-solid-state PCL-based and cross-linked PEO-based cell systems operated with high-voltage cathodes is compared in Table 1. The data of xBt-PCL-based cells clearly highlight that proper adjustment of polymer matrices paves the way for realizing improved cell performance, even without presence of any additives within the electrolyte formulations. Notably, in comparison to other reports, the introduced cross-linked PCL-based electrolytes provide better cycling stability at practical conditions (such as at higher C-rates) even against high-voltage composite cathode materials, in this way offering promising routes for future LMB applications.



- Acroolecular
Rapid Communications
www.mrc-journal.de

3. Conclusion

Following aspects of "green chemistry," PCL-based solid polymer electrolytes suitable for high-voltage LMBs were prepared, where solvent-free synthesis and membrane processing afforded intrinsically "dry" materials with improved cell safety. Cross-linked membranes (xBt-PCL) afforded better thermal and mechanical stabilities or potentially promoted bio-degradability compared to noncross-linked Bt-PCL variants, in addition to limiting inhomogeneous Li metal deposition.^[28] Notably, the cross-linking does not restrain the actual Li-ion transport within the SPEs as demonstrated by MD simulations. Dendritic/"mossy" Li deposits that eventually promote the occurrence of "voltage noise" were monitored by ⁷Li solid-state NMR, while homogeneous Li deposition could be observed for cross-linked xBt-PCL-based cells, emphasizing the beneficial impact of enhanced mechanical strength and higher Li-ion transference number to achieve better electrochemical cycling performance. Limiting current densities were also discussed, revealing reasonable potential for fast charging of the cells. Furthermore, cells operated with NMC622 cathodes that were impregnated with 1.5 wt% PCL provided reasonable initial specific discharge capacity of 121 mAh g⁻¹ and significantly improved cycling stability at rates of 1C (at 60 °C), clearly reflecting enhanced electrolyte|electrode contacts within cathode composites and lesser charge transfer limitations. Despite better cell performance compared to current high-voltage cathodes|SPEs|Li cells (Table 1), further improvements of relevant features such as ionic conductivity, capacity retention or higher cathode mass loading are required to approach all necessities for "real-world" battery applications. Here, fabrication of SPE-supported cathodes could be an approach to facilitate higher energy densities of current LMBs.

4. Experimental Section

Materials: All the materials, including ε-Caprolactone (97%, Sigma-Aldrich), phloroglucinol (≥ 99%, Sigma-Aldrich), tin(II) 2-ethylhexanoate (92.5–100.0%, Sigma-Aldrich), tetrahydrofuran (THF) (≥ 99.0%, Sigma-Aldrich), methanol (≥ 99.8%, Sigma-Aldrich), benzophenone (> 99%, TCI), lithium bis(trifluoromethanesulfonyl)imide (LiTFSI) (battery grade, 3M), LiNi_{0.6}Co_{0.2}Mn_{0.2}O₂ (NMC622) (BASF TODA Battery Materials LLC), Super C65 (Imerys Graphite & Carbon), polyvinylidene difluoride (PVdF) (Solef 5130, Solvay), *N*-methyl-2-pyrrolidone (NMP) (99.5%, Sigma-Aldrich), were purchased and used as received. Lithium metal (500 μm, Albemarle) was roll-pressed to 300 μm prior to cell assembly.

Synthesis of PCL-Based Star Polymers (Scheme 1): A predried 100 mL round-bottom flask with a magnetic stirrer was charged with ϵ -caprolactone (6.38 g, 56 mmol), phloroglucinol (0.1 g, 0.8 mmol), and tin(II) 2-ethylhexanoate (22.5 mg, 0.056 mmol). The colorless solution of \approx 6.5 mL volume was reacted at 110 °C for 24 h under Argon atmosphere. 20 mL of THF was then introduced and the dissolved polymer was added dropwise into a deionized water/methanol mixture (400 mL each). The white precipitated polymer was collected and dissolved in 20 mL of THF, then precipitated again. Finally, the polymer was collected and dried under vacuum (10^{-3} mbar) at 60 °C overnight (yield: 6.05 g, 93.4%). 1 H, 13 C NMR spectra and gel permeation chromatography (GPC) spectrum are shown in Figures S10 and S11 (Supporting Information), respectively. $M_n = 27 \ 304 \ {\rm g \ mol}^{-1}, M_w = 45 \ 008 \ {\rm g \ mol}^{-1}, D = 1.65$. (dispersity $D = {\rm weight\text{-average}}$ molar mass M_n).

Preparation of Bt-PCL and xBt-PCL Membranes (Scheme 1): All procedures were done in a dry room (dew point: < -65 °C). In a general approach, the PCL-based star polymer was dry-mixed with LiTFSI (0.3 g PCL,

0.151 g LiTFSI, [C=O]:[Li] = 5:1) on a Mylar foil (100 μ m, silicon coated, PPI Adhesive Products GmbH) at 100 °C. The mixture was then hot-pressed between two Mylar foils for three times at 100 °C at 20 bar to ensure homogeneity, prior to being sealed in a pouch bag under vacuum and aged at 80 °C overnight. Afterward, the homogenous polymer mixture was hot-pressed between two Mylar foils with a 100 μ m spacer at 80 °C, 20 bar. For xBt-PCL membranes, in addition to the above process, benzophenone as photoinitiator (4.5 wt% with respect to the polymer weight) was also added into the mixture. Upon hot-pressing, the membrane was crosslinked by UV radiation (UVACUBE 100, Dr. Hönle AG) for 7.5 min each side.

Preparation of Composite NMC622 Cathode: PVdF (0.276 g) was dissolved in NMP (10 mL) and stirred overnight at 40 °C. NMC622 (1 g, 90 wt%), Super C65 (0.077 g, 7 wt%), and 1.27 g of NMP solution (containing 3 wt% of PVdF) were loaded into a UG container (Umano) and placed in a planetary centrifugal mixer (ARM-310, THINKY), being mixed for 20 min at a speed of 1700 rpm. The slurry was subsequently casted on an aluminum foil (20 μ m, Evonik Industries) using a doctor blade with 50 μ m in gap width. The cathode sheet was dried at 80 °C overnight, followed by calendaring to a thickness of 35 μ m. Prior to use, the electrodes were punched and dried under reduced pressure (10 $^{-3}$ mbar) at 110 °C for 6 h; the mass loading was 2.5 mg cm $^{-2}$.

Materials Characterization: The experimental setup and measurement protocol of ⁷Li solid-state NMR to monitor Li deposition was employed as previously reported. [46] ¹H and ¹³C NMR spectra were recorded at a BRUKER 400 AVANCE III HD instrument using deuterated chloroform (CDCl₃) as the reference signal. DSC measurements were conducted on a Discovery DSC 2500 device (TA Instruments), where the samples (≈10 mg) were hermetically sealed in aluminum pans in a dry room. The samples were first heated up to 100 °C for 10 min and then guenched to -100 °C under helium atmosphere (flow: 50 mL min⁻¹), followed by heating up again to 100 °C with a heating rate of 10 °C min⁻¹. Rheology measurements were performed on a Physica MCR 102 rheometer (Anton Paar) equipped with a parallel-plate measuring system ($\emptyset = 15$ mm, PP15, Anton Paar). The set temperatures (40, 60 °C) were controlled by an TC 30 temperature control unit (Anton Paar). An amplitude sweep was first carried out at 0.1-10% of applied strain at a fixed frequency of 10 Hz to determine the linear viscoelastic region (LVER). For the frequency sweep, the strain value of 0.3% was used for all measurements in the range of $1-400 \text{ rad s}^{-1}$. An axial force of 1 N was applied during the whole measurement. Postmortem analysis of Li|SPE|Li cells was done by SEM (Auriga CrossBeam workstation, Zeiss, Germany), exploiting an acceleration voltage of 3 kV.

Electrochemical Investigations: All cells were assembled in a two-electrode coin cell setup (CR2032) in a dry room. [59] Ionic conductivity measurements were conducted on a Multi Autolab M204 device (Metrohm AG) within the frequency range of 1 Hz to 1 MHz. The respective polymer membrane was placed into a punched mylar foil ring (ID = 12 mm, OD = 16 mm) between two stainless steel electrodes to prevent potential short-circuit for noncross-linked SPE at temperatures that exceed its melting point. After preheating to 70 °C, a temperature-range from 10 to 70 °C was applied in steps of 10 °C. EIS measurements were performed on a VMP3 Potentiostat instrument (BioLogic) in the range between 100 mHz and 1 MHz, and an amplitude of 10 mV voltage was applied in case of asymmetric NMC622|SPE|Li cells. Lithium ion transference numbers (t_+) were determined with an VMP3 potentiostat (BioLogic) following a combined technique based on potentiostatic polarization and AC impedance measurements according to Equation (1)[60]

$$t_{+} = \frac{I_{SS} \left(\Delta V - I_{0} R_{\text{int, 0}} \right)}{I_{0} \left(\Delta V - I_{SS} R_{\text{int, SS}} \right)} \tag{1}$$

with I_0 and $I_{\rm SS}$ denoting initial and steady-state currents, $R_{\rm int,0}$ and $R_{\rm int,SS}$ denoting initial and steady-state interface resistances, respectively. Symmetric Li|SPE|Li cells were assembled and kept at open circuit for two days at 60 °C prior to impedance analysis. Afterward, impedances were measured between 1 mHz and 1 MHz, followed by applying DC polarization



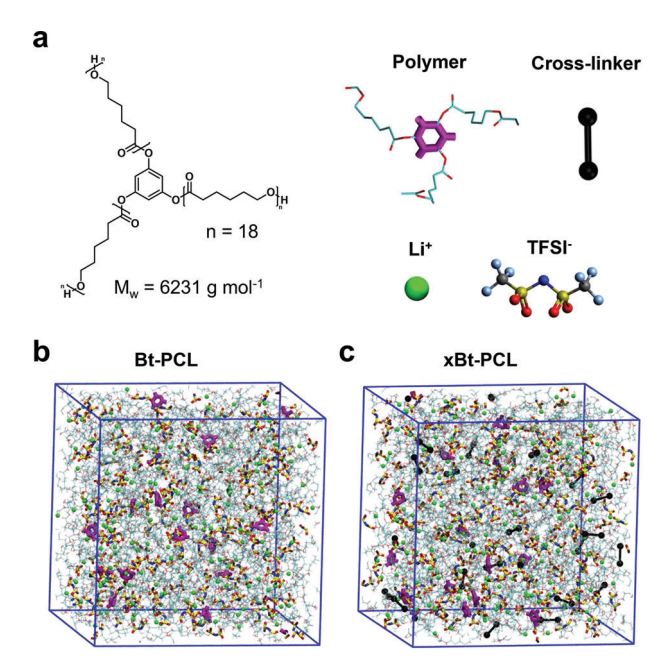


Figure 10. a) Chemical structure of BT-PCL chains used in MD simulations and representative snapshots of bulk BT-PCL b) and xBT-PCL c) systems investigated in MD simulations.

voltages of 10 mV (ΔV) until the observable current reached a steady-state value, and the impedance was measured again. Linear sweep voltammetry (LSV) was carried out on the VMP3 Potentiostat instrument (BioLogic), using lithium as counter electrode, stainless steel, or copper as working electrode for determining the anodic or cathodic stability in a two-electrode coin cell setup. A scan rate of $0.1\,\mathrm{mV}~\mathrm{s}^{-1}$ was applied in the voltage range from -0.2 to 6 V at 60 °C. Anodic stability tests against active cathode material (NMC622) was performed via galvanostatic overcharge experiments at a specific current of 0.1C (0.045 mA cm⁻²) and cut-off voltage of 6 V. Long-term galvanostatic experiments were done on Maccor devices Series 4000 (USA). The coin cells were rested inside climate chambers at constant temperature of either 60 or 40 °C for a duration of 12 h prior to cycling, in an effort to enable better contacts at the interfaces. Afterward, the cells were cycled in the voltage range from 2.8 to 4.3 V (constant current, CC), with constant voltage charging (CV) at 4.3 V to 0.05C.

Molecular Dynamics Simulations: Atomistic molecular dynamics (MD) simulations were performed using an in-house-developed simulation package and Atomistic Polarizable Potentials for Liquid, Electrolytes, and Polymers (APPLE&P) force fields, which have accurately predicted the behavior of solid polymer electrolytes. [36,61-64] All chemical bonds were constrained using the SHAKE algorithm.^[65] The temperature and pressure were controlled through the Nosé-Hoover thermostat and barostat. [66,67] A cut-off of 15.0 Å was employed to compute the van der Waals interaction and real part of electrostatic interaction, while the Ewald summation method was employed to derive the contribution from the reciprocal part of electrostatic interaction. Isotropic polarizability was assigned to each atomic center, and a Thole screening factor of 0.2 was utilized to prevent a polarizability catastrophe. $^{[68]}$ A multiple time-step integration scheme was incorporated to accelerate the simulation, with the smallest time step of 0.5 fs for bonds, bends, and improper torsional motions, a medium step of 1.5 fs for dihedrals and short-range (< 8.0 Å) nonbonded interactions, and a large step of 3 fs for remaining nonbonded interactions and reciprocal part of the Ewald summation.^[69] Each Bt-PCL chain consisted of three arms with 18 CL repeat units in each as illustrated in Figure 10a. In the initial configuration, 16 Bt-PCL chains, 172 Li+ and 172 TFSI- ions were placed randomly in a large simulation cell. To be consistent with the experiments, the ratio [C=O]:Li+ was kept constant at 5:1. The simulation box was shrunk for 50 ps to yield a density close to 1 g cm^{-3} . The system was then heated to 600 K in the NVT ensemble and run for 3 ns to allow for the polymer chains to relax. The obtained system was cooled down to 500 K, followed by an equilibration run in NPT ensemble over 5 ns. Subsequently, the system was annealed and equilibrated at lower temperatures. To build a bulk xBt-PCL system, an equilibrated system of Bt-PCL was considered in which a random carbon atom from one of the PCL arms was selected, then searched for another carbon atom within a distance of 4.5 Å that belongs to a PCL arm from a different Bt-PCL chain. When such a pair was found, an artificial harmonic spring with force constant 10 kcal \dot{mol}^{-1} \mathring{A}^{-2} and an equilibrium distance of 4.0 Å was introduced to effectively mimic a cross-link between the two PCL arms. In the xBt-PCL system, there is a total of 24 cross-links which corresponds to 4.2 wt% of initiator, that are shared by the two arms of different chains. Representative snapshots of equilibrated Bt-PCL and xBt-PCL systems are shown in Figure 10b,c. As a reference system, a pure melt of linear PCL chains each comprised of 18 monomers was also simulated. The production runs for Bt-PCL and xBt-PCL were conducted in the NPT ensemble for over 15 ns.

Supporting Information

Supporting Information is available from the Wiley Online Library or from the author.

Acknowledgements

The authors gratefully acknowledge generous support by the German Federal Ministry of Education and Research (BMBF) within the projects "FestBatt" (Grant No. 13XP0175A) "LiBEST2" (Grant No. 13XP0304A), and "LiSI" (Grant No. 13XP0224A). A.C. and D.B. acknowledge support from the project sponsored by the Army Research Laboratory under Cooperative Agreement No. W911NF-12-2-0023. The views and conclusions contained in this document are those of the authors and should not be interpreted as representing the official policies, either expressed or implied, of ARL or the U.S. Government. The U.S. Government is authorized to reproduce and distribute reprints for Government purposes not withstanding any copyright notation herein. Authors also would like to acknowledge the Center of High Performance Computing at the University of Utah for generous allocation of computation.

Open access funding enabled and organized by Projekt DEAL.

Conflict of Interest

The authors declare no conflict of interest.

Data Availability Statement

The data that support the findings of this study are available from the corresponding author upon reasonable request.

Keywords

⁷Li NMR, biodegradable polymers, cross-linking, green chemistry, highvoltage cathodes, lithium metal batteries

> Received: April 12, 2022 Revised: June 8, 2022 Published online: June 30, 2022

^[1] V. Küpers, M. Kolek, P. Bieker, M. Winter, G. Brunklaus, Phys. Chem. Chem. Phys. 2019, 21, 26084.



Rapid Communications www.mrc-journal.de

- [2] K. Xu, Chem. Rev. 2014, 114, 11503.
- [3] W. Xu, J. Wang, F. Ding, X. Chen, E. Nasybulin, Y. Zhang, J.-G. Zhang, Energy Environ. Sci. 2014, 7, 513.
- [4] H. Kim, G. Jeong, Y.-U. Kim, J.-H. Kim, C.-M. Park, H.-J. Sohn, Chem. Soc. Rev. 2013, 42, 9011.
- [5] D. Wang, W. Zhang, W. Zheng, X. Cui, T. Rojo, Q. Zhang, Adv. Sci. 2017, 4, 1600168.
- [6] X.-B. Cheng, R. Zhang, C.-Z. Zhao, F. Wei, J.-G. Zhang, Q. Zhang, Adv. Sci. 2016, 3, 1500213.
- [7] A. Manthiram, X. Yu, S. Wang, Nat. Rev. Mater. 2017, 2, 16103.
- [8] T. Placke, R. Kloepsch, S. Dühnen, M. Winter, J. Solid State Electrochem. 2017, 21, 1939.
- [9] L. Han, M. L. Lehmann, J. Zhu, T. Liu, Z. Zhou, X. Tang, C.-T. Heish, A. P. Sokolov, P. Cao, X. C. Chen, T. Saito, Front. Energy Res. 2020, 8,
- [10] L. Long, S. Wang, M. Xiao, Y. Meng, J. Mater. Chem. A 2016, 4, 10038.
- [11] J. R. Nair, L. Imholt, G. Brunklaus, M. Winter, Electrochem. Soc. Interface 2019, 28, 55.
- [12] A. Manuel Stephan, K. S. Nahm, Polymer 2006, 47, 5952.
- [13] J. Mindemark, M. J. Lacey, T. Bowden, D. Brandell, Prog. Polym. Sci. 2018. 81. 114.
- [14] O. Buriez, Y. B. Han, J. Hou, J. B. Kerr, J. Qiao, S. E. Sloop, M. Tian, S. Wang, J. Power Sources 2000, 89, 149.
- [15] E. Strauss, S. Menkin, D. Golodnitsky, J. Solid State Electrochem. 2017, 21, 1879.
- [16] I. Cekic-Laskovic, N. Von Aspern, L. Imholt, S. Kaymaksiz, K. Oldiges, B. R. Rad, M. Winter, Top. Curr. Chem. Cham 2017, 375, 37.
- [17] G. Homann, L. Stolz, J. Nair, I. C. Laskovic, M. Winter, J. Kasnatscheew, Sci. Rep. 2020, 10, 4390.
- [18] G. Homann, L. Stolz, M. Winter, J. Kasnatscheew, Iscience 2020, 23, 101225.
- [19] S. Dühnen, J. Betz, M. Kolek, R. Schmuch, M. Winter, T. Placke, Small Methods 2020, 4, 2000039.
- [20] C. P. Fonseca, D. S. Rosa, F. Gaboardi, S. Neves, J. Power Sources 2006, 155, 381.
- [21] P.-M. Jalbert, B. Commarieu, J.-C. Daigle, J. P. Claverie, K. Zaghib, J. Electrochem. Soc. 2020, 167, 080527.
- [22] M. P. Rosenwinkel, R. Andersson, J. Mindemark, M. Schönhoff, J. Phys. Chem. C 2020, 124, 23588.
- [23] P. Barai, K. Higa, V. Srinivasan, Phys. Chem. Chem. Phys. 2017, 19, 20493.
- [24] C. Polo Fonseca, S. Neves, J. Power Sources 2006, 159, 712.
- [25] Y. Li, M. Liu, S. Duan, Z. Liu, S. Hou, X. Tian, G. Cao, H. Jin, ACS Appl. Energy Mater. 2021, 4, 2318.
- [26] H. Xu, W. Ye, Q. Wang, B. Han, J. Wang, C. Wang, Y. Deng, J. Mater. Chem. A 2021, 9, 9826.
- [27] K. S. Ngai, S. Ramesh, K. Ramesh, J. C. Juan, *Ionics* 2016, 22, 1259.
- [28] C. Kósa, M. Sedlačík, A. Fiedlerová, Š. Chmela, K. Borská, J. Mosnáček, Eur. Polym. J. 2015, 68, 601.
- [29] J. R. Nair, I. Shaji, N. Ehteshami, A. Thum, D. Diddens, A. Heuer, M. Winter, Chem. Mater. 2019, 31, 3118.
- [30] S. Chen, J. Wang, Z. Wei, Z. Zhang, Y. Deng, X. Yao, X. Xu, J. Power Sources 2019, 431, 1.
- [31] W. Choi, Y. Kang, I.-J. Kim, B.-G. Seong, W.-R. Yu, D. W. Kim, ACS Appl. Mater. Interfaces 2021, 13, 35664.
- [32] B. Commarieu, A. Paolella, S. Collin-Martin, C. Gagnon, A. Vijh, A. Guerfi, K. Zaghib, J. Power Sources 2019, 436, 226852.
- [33] C.-K. Lin, I.-D. Wu, Polymer 2011, 52, 4106.
- [34] M. Marzantowicz, J. R. Dygas, F. Krok, J. L. Nowiński, A. Tomaszewska, Z. Florjańczyk, E. Zygadło-Monikowska, J. Power Sources 2006, 159, 420.

- [35] H. Xu, J. Xie, Z. Liu, J. Wang, Y. Deng, MRS Energy Sustainability 2020, 7. 2.
- [36] D. Dong, A. Choudhary, D. Bedrov, ACS Appl. Polym. Mater. 2020, 2, 5358
- [37] F. M. Gray, in Solid State Electrochemistry (Ed: P. G. Bruce), Cambridge University Press, Cambridge 1994, pp. 119-162.
- [38] M. P. Rosenwinkel, M. Schönhoff, J. Electrochem. Soc. 2019, 166, A1977.
- [39] M. S. Grewal, M. Tanaka, H. Kawakami, Polym. Int. 2019, 68, 684.
- [40] A. Franck, T. I. Germany, Viscoelasticity and Dynamic Mechanical Testing, TA Instruments, New Castle, DE 1993.
- [41] C. Monroe, J. Newman, J. Electrochem. Soc. 2005, 152, A396.
- [42] R. Khurana, J. L. Schaefer, L. A. Archer, G. W. Coates, J. Am. Chem. Soc. 2014, 136, 7395.
- [43] J. Lopez, D. G. Mackanic, Y.i Cui, Z. Bao, Nat. Rev. Mater. 2019, 4,
- [44] C. Brissot, M. Rosso, J.-N. Chazalviel, P. Baudry, S. Lascaud, Electrochim. Acta 1998, 43, 1569.
- [45] C. Brissot, M. Rosso, J.-N. Chazalviel, S. Lascaud, J. Power Sources **1999**, *81–82*, 925.
- [46] Y.-C. Hsieh, M. Leißing, S. Nowak, B.-J. Hwang, M. Winter, G. Brunklaus, Cell Rep. Phys. Sci. 2020, 1, 100139.
- [47] H. J. Chang, N. M. Trease, A. J. Ilott, D. Zeng, L.-S. Du, A. Jerschow, C. P. Grey, J. Phys. Chem. C 2015, 119, 16443.
- [48] T. O'Haver, peakfit.m., https://www.mathworks.com/matlabcentral/ fileexchange/23611-peakfit-m, (accessed: January 2018).
- [49] R. Bhattacharyya, B. Key, H. Chen, A. S. Best, A. F. Hollenkamp, C. P. Grey, Nat. Mater. 2010, 9, 504.
- [50] J.-N. Chazalviel, Phys. Rev. A 1990, 42, 7355.
- [51] K. Borzutzki, K. Dong, J. R. Nair, B. Wolff, F. Hausen, R.-A. Eichel, M. Winter, I. Manke, G. Brunklaus, Cell Rep. Phys. Sci. 2021, 2, 100496.
- [52] G. Bieker, M. Winter, P. Bieker, Phys. Chem. Chem. Phys. 2015, 17, 8670
- [53] M. Rosso, C. Brissot, A. Teyssot, M. Dollé, L. Sannier, J. -. M. Tarascon, R. Bouchet, S. Lascaud, Electrochim. Acta 2006, 51, 5334.
- [54] M.ickaël Dollé, L. Sannier, B. Beaudoin, M. Trentin, J. -. M. Tarascon, Electrochem. Solid State Lett. 2002, 5, A286.
- [55] A. Gupta, E. Kazyak, N. Craig, J. Christensen, N. P. Dasgupta, J. Sakamoto, J. Electrochem. Soc. 2018, 165, A2801.
- [56] S. Chen, C. Niu, H. Lee, Q. Li, L. Yu, W. Xu, J.-G. Zhang, E. J. Dufek, M. S. Whittingham, S. Meng, J. Xiao, J. Liu, Joule 2019, 3, 1094.
- [57] K. Borzutzki, M. Winter, G. Brunklaus, J. Electrochem. Soc. 2020, 167, 070546.
- [58] W. Cai, Y. Zhang, J. Li, Y. Sun, H. Cheng, Chem Sus Chem 2014, 7, 1063.
- [59] R. Nölle, K. Beltrop, F. Holtstiege, J. Kasnatscheew, T. Placke, M. Winter, Mater. Today 2020, 32, 131.
- [60] J. Evans, C. A. Vincent, P. G. Bruce, Polymer 1987, 28, 2324.
- [61] D. Bedrov, J.-P. Piquemal, O. Borodin, A. D. Mackerell, B. Roux, C. Schröder, Chem. Rev. 2019, 119, 7940.
- [62] O. Borodin, J. Phys. Chem. B 2009, 113, 11463.
- [63] K. Borzutzki, D. Dong, C. Wölke, M. Kruteva, A. Stellhorn, M. Winter, D. Bedrov, G. Brunklaus, iScience 2020, 23, 101417.
- [64] C. H. Krause, A. J. Butzelaar, D. Diddens, D. Dong, P. Théato, D. Bedrov, B.-J. Hwang, M. Winter, G. Brunklaus, J. Power Sources 2021, 484, 229267.
- [65] B. J. Palmer, J. Comput. Phys. 1993, 104, 470.
- [66] D. J. Evans, B. L. Holian, J. Chem. Phys. 1985, 83, 4069.
- [67] W. G. Hoover, Phys. Rev. A 1985, 31, 1695.
- [68] B. T. Thole, Chem. Phys. 1981, 59, 341.
- [69] G. J. Martyna, M. E. Tuckerman, D. J. Tobias, M. L. Klein, Mol. Phys. 1996, 87, 1117.